Using Large Eddy Simulation within an Acoustic Analogy Approach for Jet Noise Modelling

S.A. Karabasov[1], M.Z. Afsar[2], T.P. Hynes[3], A.P. Dowling[4]
University of Cambridge, Cambridge, UK

W.A. McMullan[5], C.D. Pokora[6], G.J. Page[7], and J.J. McGuirk[8]
Loughborough University, Loughborough, UK

A novel approach to the development of a hybrid prediction methodology for jet noise is described. Modelling details and numerical techniques are optimised for each of the three components of the model individually. Far field propagation is modelled via solution of a system of adjoint Linear Euler Equations, capturing convective and refraction effects via use of a spatially developing jet mean flow provided by a RANS CFD solution. Sound generation is modelled following Goldstein's acoustic analogy, including a Gaussian function model for the two-point cross-correlation of the 4th order velocity fluctuations in the acoustic source. Parameters in this model describing turbulent length- and time-scales are assumed to be proportional to turbulence information taken also from the RANS CFD prediction. The constants of proportionality are, however, not determined empirically, but extracted via comparison with turbulence length- and time-scales obtained from an LES prediction. The LES results are shown to be in good agreement with experimental data for the 4th order two-point cross-correlation functions. The LES solution is then used to determine the amplitude parameter and also to examine which components of the cross-correlation are largest, enabling inclusion of all identified dominant terms in the Gaussian source model. The acoustic source description in the present approach is therefore determined with no direct input from experimental data. The paper also examines the accuracy of various commonly made simplifications, for example: the inclusion of an evolving jet flow and scattering from the nozzle, the assumption of small variation in Green's function over the correlation length, the application of the far-field approximation in the Green's function, and the impact of isotropic assumptions made in previous acoustic source models. The final optimised model is applied to prediction of experimental data from the JEAN project, and gives excellent agreement across a wide spectral range and for both sideline and peak noise angles.

I. Introduction

DEVELOPMENTS of the original acoustic analogy proposed by Lighthill[1] remain a major tool for the prediction of jet noise. By an exact re-arrangement of the Navier Stokes equations, Lighthill[1] showed that the noise from a turbulent jet could be viewed as a distribution of quadrupole sources in the acoustic wave equation, the strength of the quadrupoles, T_{ij}, depending primarily on the local fluctuating Reynolds stresses, $\rho v_i' v_j'$. The turbulent eddies which give rise to the Reynolds stresses are convected by the jet velocity and their motion alters the radiated sound, an effect correctly accounted for by Ffowcs Williams[2]. The mean jet velocity has yet another influence: it refracts the sound [3, 4] altering the propagation of sound from the sources to the far field. Lilley's approach [5] was to describe

[1] Royal Society University Research Fellow, Department of Engineering, AIAA member.
[2] PhD Student, Department of Engineering, AIAA student member.
[3] Senior Lecturer in fluid mechanics, Department of Engineering.
[4] Professor of Mechanical Engineering, Department of Engineering, AIAA member.
[5] Post-Doctoral Research Associate, Department of Aeronautical and Automotive Engineering.
[6] PhD Student, Department of Aeronautical and Automotive Engineering.
[7] Senior Lecturer, Department of Aeronautical and Automotive Engineering. AIAA Member.
[8] Professor of Aerodynamics, Department of Aeronautical and Automotive Engineering.

this propagation through a specified mean flow velocity profile, taken to be a function of radius only. This is clearly restrictive, introducing sensitivity to the axial station chosen for matching the velocity profile [6].

Goldstein's formulation [7], which will be used in this paper, re-arranges the Navier-Stokes equations into Linearised Euler Equations (LEE) (involving the evolving mean jet flow) for the propagating quantities with non-linear terms representing the analogous acoustic sources. Because the true evolving mean jet flow is used, the convection effects on acoustic sources and the refraction effects on the sound are correctly captured. The sound field can then be represented using an adjoint Green function solution of the LEE together with a model or calculation of the statistics of the source terms [8]. Because the Linearised Euler Equations are also those which govern shear flow instability, it is important, as pointed out by Argawal et al.[9], to avoid contamination by shear flow instabilities. This can be accomplished by solving the LEE in the frequency domain provided the method of iteration is carefully chosen [10].

In a number of previous investigations of jet noise [11, 12], a statistically stationary Reynolds-Averaged Navier Stokes (RANS) solution for the jet flowfield, incorporating a k-ε turbulence model, has been used to determine the underlying mean flow, and to provide statistical (time-averaged) turbulence information which was used to characterise the acoustic sources. The two-point space-time correlation function of the acoustic sources was estimated via an assumed model function, whose amplitude and integral length and time scales were deduced from the predicted turbulence information via empirically determined relationships. Tam and Auriault[12] introduced a model through an heuristic argument based on an analogy between molecular pressure, from the kinetic theory of gases, and the turbulent pressure from fine scale turbulence. Morris and Farassat[13] showed this to be equivalent to an acoustic analogy provided one represents the source and Green function consistently.

Sound predictions based upon source statistics derived from RANS calculations under the assumption that the turbulent Reynolds stresses, T_{ij}, are isotropic everywhere and at all times give good predictions of the higher frequency sound that dominates at 90^0 to the jet axis (the important side-line condition in aircraft certification) and in the forward arc[12]. However, this approach gives a significant under prediction in the rearward arc, where sound is of lower frequency and comes from larger-scale coherent structures in the jet[13]. Afsar et al.[14] argued that a more realistic model of this type would be to assume that the turbulence is only statistically isotropic i.e. that the temporal-spatial (2-point, 2-time) cross-correlation of the turbulent sources is isotropic rather than T_{ij}, itself.

The turbulent statistics associated with large-scale coherent structures, potentially contributing to low frequency sound, appear amenable to calculation by more advanced methods. In this paper we will use Large Eddy Simulation (LES) CFD of a jet to generate these. By comparison with those obtained from RANS CFD, we aim to develop better source models, which rely on less empiricism for correlation scales and which are valid for a much wider range of frequencies. In section II, we describe the acoustic analogy, source representation theorem and Green function method. Section III provides a description of the LES method and its comparison with experimental data, together with the prediction of acoustic source statistics. Models of these statistics are developed in section IV and used to infer the far field sound that is compared with experiment.

II. Representation of acoustic field

Following Goldstein[7] , we decompose the flow variables for density, pressure, velocity and enthalpy into a steady mean and unsteady perturbation of the form

$$\rho = \overline{\rho} + \rho' \qquad p = \overline{p} + p' \qquad v_i = \tilde{v}_i + v_i'' \qquad h = \tilde{h} + h''$$

where $\overline{(\,)}$ represents a time average, $\widetilde{(\,)}$ a Favre average and single and double primes represent the corresponding variation about the mean. The unsteady Navier Stokes equations can then be re-arranged into Linearised Euler terms on the left hand side operating on perturbation variables equal to simple non-linear source terms on the right. These are, with position and time represented by $(\mathbf{y}, \tau)$,

$$
\begin{aligned}
&\frac{\partial \rho'}{\partial \tau}+\frac{\partial}{\partial y_j}(\rho'\tilde{v}_j+u_j)=0\\
&\frac{\partial u_i}{\partial \tau}+\frac{\partial}{\partial y_j}(\tilde{v}_j u_i)+\frac{\partial p'}{\partial y_i}+u_j\frac{\partial \tilde{v}_i}{\partial y_j}-\left(\frac{\rho'}{\bar{\rho}}\right)\frac{\partial \tilde{\tau}_{ij}}{\partial y_j}=\frac{\partial T'_{ij}}{\partial y_j}\quad i=1,..3.\\
&\left(\frac{1}{\gamma-1}\right)\frac{\partial p'}{\partial \tau}+\left(\frac{1}{\gamma-1}\right)\frac{\partial}{\partial y_j}(p'\tilde{v}_j)+\frac{\partial}{\partial y_j}(u_j\tilde{h})+p'\frac{\partial \tilde{v}_j}{\partial y_j}-\left(\frac{u_i}{\bar{\rho}}\right)\frac{\partial \tilde{\tau}_{ij}}{\partial y_j}=Q.
\end{aligned}
\tag{1}
$$

In this formulation, a momentum pertubation variable is defined (with zero time average) as $u_i=\rho v_i''$; and the Favre averaged stagnation enthalpy, and its perturbation, take the special definitions:

$$
\tilde{h}_o=\tilde{h}+\frac{1}{2}\tilde{v}^2\quad\text{and}\quad h_o''=h''+\tilde{v}_i v_i''+\frac{1}{2}v''^2.
\tag{2}
$$

The source terms are:

$$
T'_{ij}=-(\rho v_i''v_j''-\bar{\rho}\widetilde{v_i''v_j''})
\tag{3}
$$

$$
Q=-\tilde{v}_j\frac{\partial T'_{ij}}{\partial y_i}+\frac{1}{2}\delta_{ij}\left[\frac{DT'_{ij}}{D\tau}+\frac{\partial \tilde{v}_k}{\partial y_k}T'_{ij}\right]-\frac{\partial}{\partial y_j}\left(\rho v_j''h_o''-\bar{\rho}\widetilde{v_j''h_o''}\right)
\tag{4}
$$

where $D/D\tau$ is the convective derivative, $\dfrac{D}{D\tau}=\dfrac{\partial}{\partial \tau}+\tilde{v}_j(\mathbf{y})\dfrac{\partial}{\partial y_j}$.

For the unheated jets considered in this paper, we will asssume that the last term in equation (4) is negligible. With this approximation, *Q* reduces to:

$$
Q=-\tilde{v}_j\frac{\partial T'_{ij}}{\partial y_i}+\frac{1}{2}\delta_{ij}\left[\frac{DT'_{ij}}{D\tau}+\frac{\partial \tilde{v}_k}{\partial y_k}T'_{ij}\right]
\tag{5}
$$

The wave propagation problem is solved in the frequency domain using an adjoint Green function method. $\hat{\mathbf{G}}(\mathbf{y},\omega\,|\,\mathbf{x})$, the Fourier transform of the adjoint Green function, satisfies the adjoint equations:

$$
\begin{aligned}
&i\omega\hat{G}_o+\tilde{v}_j\frac{\partial \hat{G}_o}{\partial y_j}+\left(\frac{\hat{G}_i}{\bar{\rho}}\right)\frac{\partial \tilde{\tau}_{ij}}{\partial y_j}=0\\
&i\omega\hat{G}_j+\frac{\partial \hat{G}_o}{\partial y_j}+\tilde{v}_i\frac{\partial \hat{G}_j}{\partial y_i}-\hat{G}_i\frac{\partial \tilde{v}_i}{\partial y_j}+\tilde{h}\frac{\partial \hat{G}_4}{\partial y_j}+\left(\frac{\hat{G}_4}{\bar{\rho}}\right)\frac{\partial \tilde{\tau}_{ij}}{\partial y_i}=0\quad j=1,..3.\\
&\left(\frac{i\omega}{\gamma-1}\right)\hat{G}_4+\left(\frac{\tilde{v}_j}{\gamma-1}\right)\frac{\partial \hat{G}_4}{\partial y_j}-\hat{G}_4\frac{\partial \tilde{v}_j}{\partial y_j}+\frac{\partial \hat{G}_j}{\partial y_j}=\delta(\mathbf{y}-\mathbf{x}).
\end{aligned}
\tag{6}
$$

In the adjoint formulation, the unit point source in equation (6) is at **x**, the position of the observer, and is generally at some distance from the jet. $\hat{G}_o$ is the adjoint density-like variable and $\hat{G}_1$ - $\hat{G}_3$ are the adjoint momentum-like variables. $\hat{G}_4$, the pressure-like quantity, is the variable in the adjoint energy equation.

For axisymmetric jets, it is convenient to express $\hat{\mathbf{G}}$ as the sum of a free-space solution for a point source at **x** (which is known analytically) and a scattered field due to the presence of the jet in the manner of Tam & Auriault[8]

$$\hat{\mathbf{G}} = \hat{\mathbf{G}}_{\text{free-space}} + \hat{\mathbf{G}}_{\text{scattered}}. \tag{7}$$

The scattered field is found as a sum of circumferential harmonics by numerical solution of equation (6), for each harmonic, using a finite volume version of a modified Adams scheme, which uses carefully adjusted dual-scale iterative time stepping to stabilise the effects of large shear gradient terms and to avoid contamination by the shear layer instability[10]. When the observer position **x** is at a large distance from the jet, the spatial dependence of $\hat{\mathbf{G}}_{\text{free-space}}$ on **y** takes the form of the *n*'th circumferential harmonic of a plane wave[8]. For comparison with the experiments that are described in section IV, where the acoustic measurements were taken at 30 diameters from the jet, the spatial dependence of $\hat{\mathbf{G}}_{\text{free-space}}$ includes the next term in $r/|\mathbf{x}|$, where *r* is the radial component of **y** [10].

The underlying mean flow for the linearised solution was extracted from a RANS solution obtained on a mesh carefully designed to maximise the quality of the Green function solution. The solution domain includes the nozzle and is terminated at a large downstream distance using a sponge zone[10]. The boundary condition on $\hat{\mathbf{G}}$ at large distances from the jet is chosen to ensure that no surface terms appear in the representation formula for the desired flow variables.

It is relatively straightforward to formulate a representation theorem for the far field pressure in terms of the Green function and source terms. The sum of the inner products of $\hat{\mathbf{G}}$ with equation (1) and the perturbation variables with equation (5) is integrated over the region of non-zero sources. The expression obtained for the far field pressure is:

$$\hat{p}(\mathbf{x},\omega) = -\int_{V_\infty(\mathbf{y})} \left(\hat{G}_i(\mathbf{y},\omega \mid \mathbf{x}) \frac{\partial \hat{T}'_{ij}}{\partial y_j}(\mathbf{y},\omega) + \hat{G}_4(\mathbf{y},\omega \mid \mathbf{x}) \hat{Q}(\mathbf{y},\omega) \right) d^3\mathbf{y} \tag{8}$$

where $\hat{T}'_{ij}(\mathbf{y},\omega)$ and $\hat{Q}(\mathbf{y},\omega)$ are the Fourier transform of the source terms. After expanding $\hat{Q}(\mathbf{y},\omega)$ as in equation (6) and integration by parts, we obtain

$$\hat{p}(\mathbf{x},\omega) = \int_{V_\infty(\mathbf{y})} \hat{I}_{ij}(\mathbf{y},\omega \mid \mathbf{x}) \hat{T}'_{ij}(\mathbf{y},\omega) d^3\mathbf{y} \tag{9}$$

where the components of the second rank wave propagation tensor, $\hat{I}_{ij}$, are defined by:

$$\hat{I}_{ij}(\mathbf{y},\omega\,|\,\mathbf{x}) = \frac{\partial \hat{G}_j}{\partial y_i}(\mathbf{y},\omega\,|\,\mathbf{x}) - \left[\frac{\partial \tilde{v}_j}{\partial y_i}(\mathbf{y})\hat{G}_4(\mathbf{y},\omega\,|\,\mathbf{x}) + \tilde{v}_j(\mathbf{y})\frac{\partial \hat{G}_4}{\partial y_i}(\mathbf{y},\omega\,|\,\mathbf{x})\right]$$

$$+ \quad \frac{\delta_{ij}}{2}\left[i\omega\left(1+\frac{\tilde{v}_k}{i\omega}\frac{\partial}{\partial y_k}\right)\hat{G}_4(\mathbf{y},\omega\,|\,\mathbf{x}) - \frac{\partial \tilde{v}_k}{\partial y_k}(\mathbf{y})\hat{G}_4(\mathbf{y},\omega\,|\,\mathbf{x})\right]. \tag{10}$$

Finally, the power spectral density of the distant sound field

$$\hat{P}(\mathbf{x},\omega) = \int_{V_\infty(\mathbf{y})}\int_{\Delta}\hat{R}_{ij,kl}(\mathbf{y},\boldsymbol{\Delta},\omega)\hat{I}_{ij}(\mathbf{y},-\omega\,|\,\mathbf{x})\hat{I}_{kl}(\mathbf{y}+\boldsymbol{\Delta},\omega\,|\,\mathbf{x})\,d^3\boldsymbol{\Delta}\,d^3\mathbf{y} \tag{11}$$

where $\hat{R}_{ijkl}(\mathbf{y},\boldsymbol{\Delta},\omega)$ is the Fourier transform of the temporal-spatial (2-point, 2-time) cross-correlation of the turbulent sources:

$$\hat{R}_{ijkl}(\mathbf{y},\boldsymbol{\Delta},\omega) = \int R_{ijkl}(\mathbf{y},\boldsymbol{\Delta},\tau)e^{-i\omega\tau}\,d\tau = \int \overline{T'_{ij}(\mathbf{y},t)T'_{kl}(\mathbf{y}+\boldsymbol{\Delta},t+\tau)}e^{-i\omega\tau}\,d\tau. \tag{12}$$

III. LES/RANS modelling

The governing Navier-Stokes equations are spatially filtered to give the LES form, which then requires a subgrid scale (sgs) model to define the unknown subgrid scale stresses. The equations are solved using a finite-volume cell-centred spatial discretisation on hexahedral elements. The elements are defined using a structured mesh multiblock formulation. This allows the capture of reasonably complex geometry (for example engine pylons or chevrons) whilst being computationally efficient.

The spatial discretisation is implemented as a family of schemes ranging from central differencing through first order upwind to high order upwind, with a single controlling parameter. In this work a second order upwind scheme is used as a compromise between numerical robustness and acceptable dispersion and dissipation characteristics. The generic upwind scheme is applied to the mass, momentum and energy equations. These equations are solved in a sequential manner with a spatially implicit scheme. The mass equation is transformed into an equation for pressure-correction to allow the computation of very low speed and truly incompressible flows without any extra numerical treatments such as pre-conditioning. Temporal advancement is by a first order backward Euler implicit scheme or a low storage Runge-Kutta third order (three stage) or fourth order (five stage) scheme. The subgrid scale model used is the standard Smagorinsky formulation with a Van Driest damping treatment to limit the length scale in the high aspect ratio cells in the near wall viscous affected region.

The baseline methodology has been tested for steady state RANS solutions for both high speed compressible flows with shock waves, and low speed incompressible problems (Page et al [15]). The Large Eddy Simulation capability was originally developed for the prediction of multiple impinging jets (Page et al [16]). The use of a multiblock formulation means that the algorithm is easily amenable to parallelisation in both shared memory or message passing formulations. These calculations were run with each block allocated to a single processor on an MPI based compute cluster.

The 3D computational grid used in the LES and RANS calculations has a total of 17 million cells and has an extent of 30*D* x 10*D* in the axial and radial directions downstream of the nozzle exit. The jet nozzle wall geometry is included in the domain and extends 5*D* upstream of the nozzle exit. 2.4 million cells, separated into two blocks, are located inside the nozzle, with the grid refined near the nozzle walls to produce a first cell height of $y+ \sim 30$. A further 2.6 million cells are placed in the region between the outer wall of the nozzle and the computational domain boundary upstream of the nozzle exit. Images of the mesh, including a close-up around the nozzle exit are shown in Figure 1, which also indicates the mesh design to provide high resolution in the jet shear layer region. Downstream of the nozzle exit, the 314 x 102 x 360 grid (axial x radial x circumferential) is partitioned into seven blocks, sliced normal to the jet axis.

The simulated flow is an isothermal Mach 0.75 round jet with a Reynolds number of 10^6, based on the jet exit velocity and the nozzle diameter (based on Power et al [17]). A constant total pressure condition is specified at nozzle

inlet to set the correct jet Reynolds and Mach numbers. A fixed static pressure outlet condition at the downstream boundary is used in both the RANS and LES calculations. In the RANS solution, the k-ε turbulence model is used with an inlet turbulence level ($k^{1/2}$/Ujet) of 1% and a length scale of 0.01*D*, as would be typical of a low turbulence plenum flow supplying a jet. This solution is annotated as RANS A in the figures below. For the LES prediction, the nozzle inlet flow has Gaussian random noise applied to the velocity field equivalent to a turbulence level of 10%. Due to the uncorrelated nature of this disturbance and the acceleration in the nozzle, this rapidly decays to very low levels in the potential core of the jet. The Smagorinsky model coefficient (CS) is set to 0.15, and we have found little sensitivity of the solution to the value of this coefficient. The LES simulation is first run for 100,000 time steps, so that the initial conditions have passed through the domain and a statistically stationary flow-field is obtained. To gather statistical data and information required to produce the 2nd- and 4th-order correlations, the simulation is then run for a further 100,000 time steps; during this time the entire flow-field is sampled at intervals of 40 LES time steps. Within each 40 time step window, a filter is applied that is designed to attenuate fluctuations with two or less sub-samples per wavelength. The file-size of the filtered flow solution at each time step is ~450MB, and up to 1TB of data is produced by the sampling procedure, rendering the extraction, processing and construction of two-point two-time correlations from the stored data very time-consuming, requiring perhaps days of computational effort in its own right.

In addition to the simulations performed with the internal Loughborough CFD solver a further RANS k-ε solution was obtained using the commercial CFD product Fluent 6.2. This calculation is performed on a different grid with 271x120 cells (axial x radial) and had a somewhat smaller domain of 20*D* x 5*D* in the axial and radial directions. This calculation was started at the nozzle exit, with a prescribed inlet turbulence level ($k^{1/2}$/Ujet) set at 6% according to the ERCOFTAC guidelines[18]. This solution, which is denoted as RANS B, has a higher level of inlet turbulence and is a better match to the experimental inlet turbulence than the RANS A solution, which like the LES was started 5 jet diameters *D* upstream of the exit nozzle.

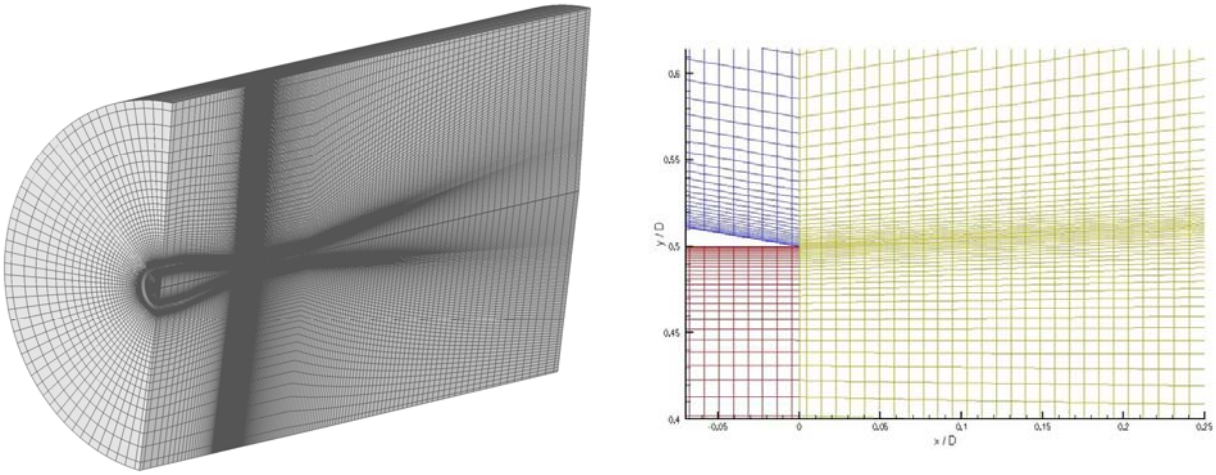

Figure 1. Mesh distribution: whole domain and near the nozzle lip for the LES/RANS A cases

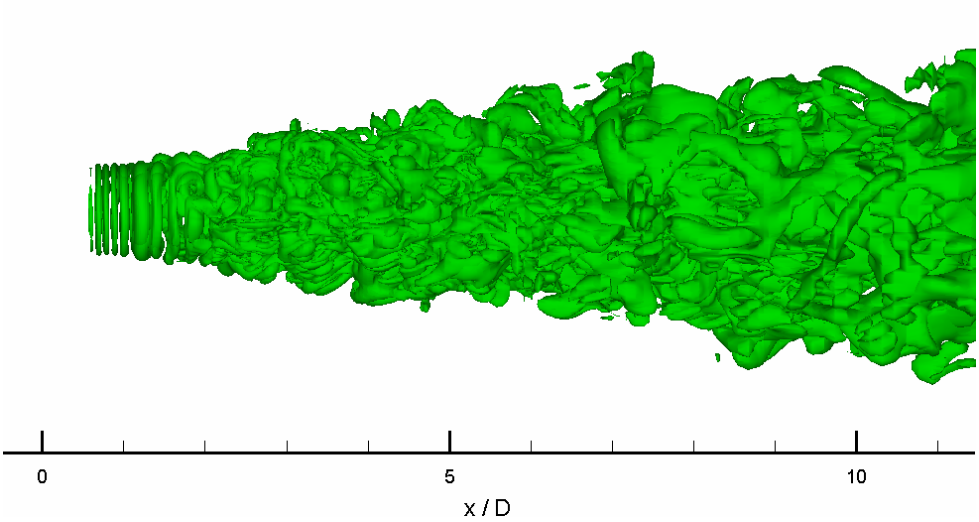

Figure 2. LES predicted instantaneous iso-surface of vorticity

The unsteady motions in the turbulent jet that are not present in the RANS calculations but are captured by the LES, are illustrated in Figure 2, which displays an iso-surface of vorticity. This picture shows that the Gaussian noise prescribed at nozzle inlet, and the subsequent boundary layer growth predicted on the internal nozzle wall in the current LES prediction, does not provide fully turbulent conditions at the nozzle exit lip for initial shear layer development. These are rather transitional, with vortex rings that break down rapidly into 3D turbulent structures. Radial profiles predicted at x/D = 1, 5 are shown in Figure 3. At x/D = 1 the statistics from all simulations are in good agreement with the experimental data. The LES prediction has a thinner shear layer than in both RANS solutions At x/D = 5 the LES somewhat over-predicts the turbulent kinetic energy in the flow, whereas the larger turbulence level predicted at nozzle exit in the RANS B case yields an improvement when compared to the RANS A case. This benefit is again clear in the statistical properties recorded along the jet centerline in Figure 4 – the higher initial k value in the RANS B case, and associated enhanced spreading, causes a reduction in the predicted potential core length, in closer agreement with measurements, whilst the RANS A case over-predicts this length by some 20%. The LES prediction under-predicts the potential core length slightly, but is capable of capturing the irrotational fluctuations measured within the potential core.

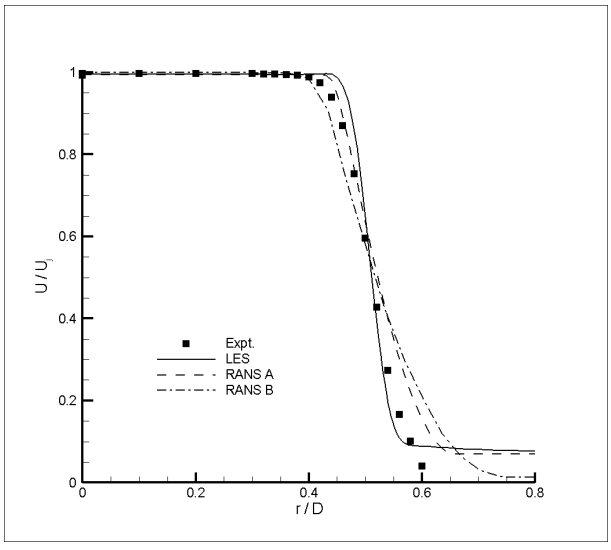

(a) x/D=1; axial velocity

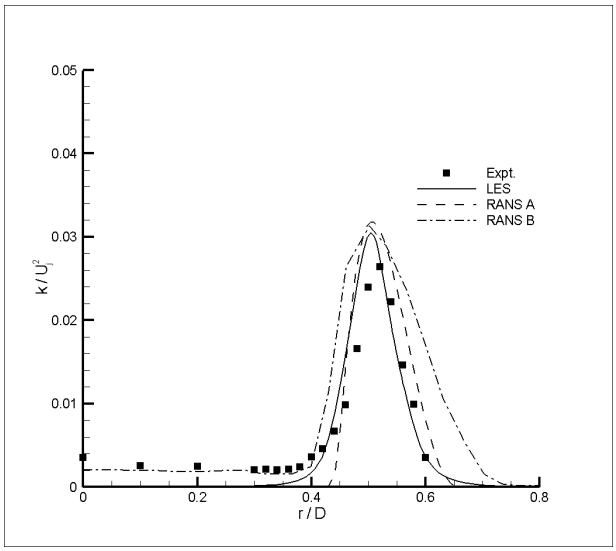

(b) x/D=1; turbulence kinetic energy

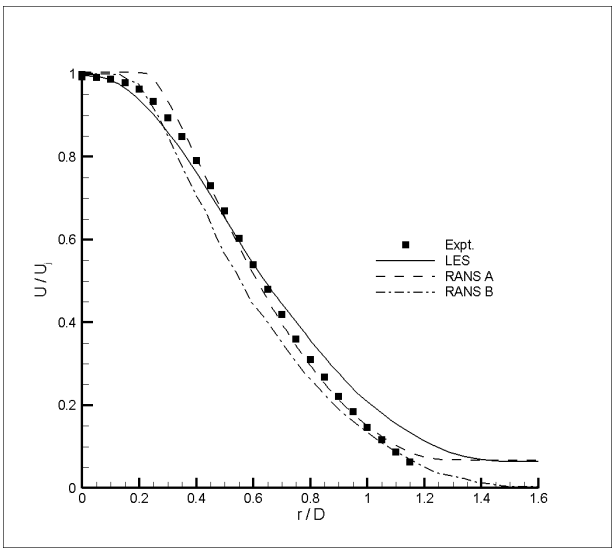

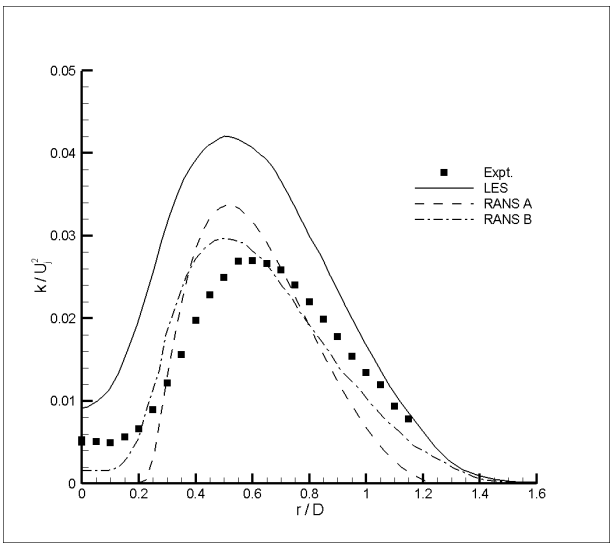

(c) x/D=5; axial velocity (d) x/D=5; turbulence kinetic energy

Figure 3. Radial profiles of axial velocity and turbulence kinetic energy

To obtain the temporal-spatial correlation functions from the LES predictions, the flow files sampled as described above are processed using custom-written software (Hollis[19]). The 2nd- and 4th- order two-point two-time correlations for the streamwise velocity fluctuation and for a streamwise separation vector (extracted from the LES at a point in the middle of the shear layer at x/D = 4) are compared with the hot-wire experimental data of Harper-Bourne[20] in Figure 5. The shape and decay of the curves are in very good agreement with the experimental data. In particular, the agreement of the 4th - order correlation is very encouraging, implying that the current simulation has captured the salient flow physics of the jet turbulence which describe the acoustic sources. It is this information that should prove most useful if it can be incorporated into the acoustic analogy model.

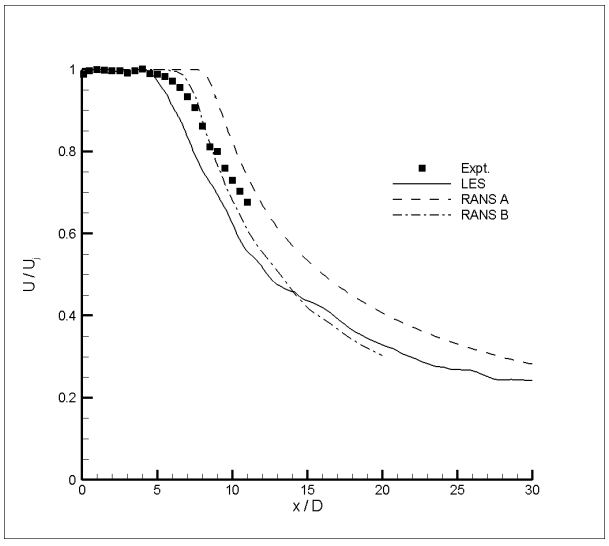

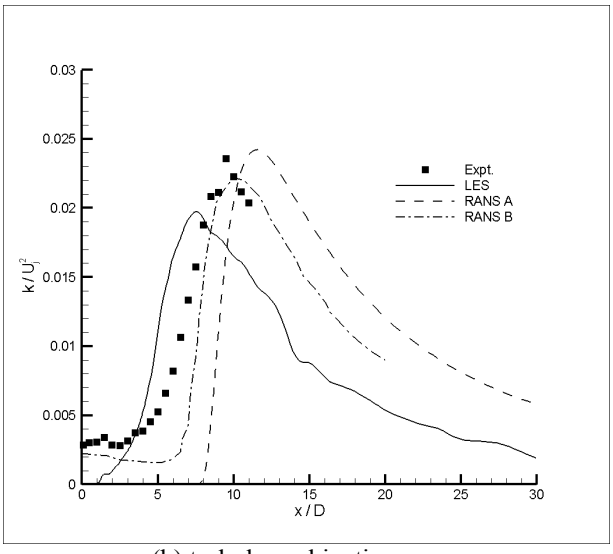

(a) axial velocity (b) turbulence kinetic energy

Figure 4. Jet centerline distributions

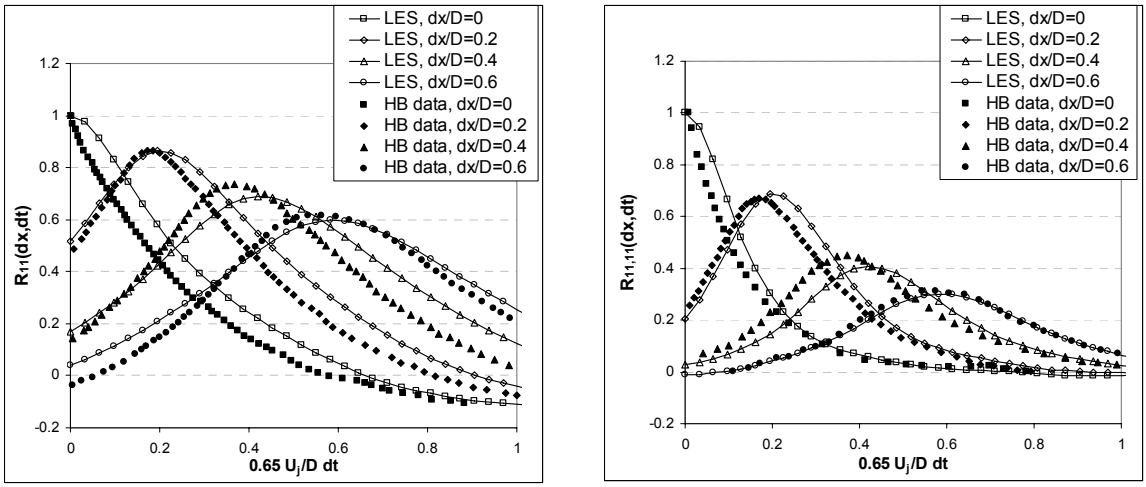

(a) (b)

Figure 5. Comparison between LES predicted correlation functions against Harper-Bourne[20] measurements 2nd-order - (a), 4th-order - (b)

It is encouraging to note that the LES predictions shown in Figure 5 were extracted from a prediction at a jet Reynolds number of 10^6 and Mach number of 0.75, whereas the Harper-Bourne[20] experiments were conducted at Re= 2x 10^5 and M = 0.18; this provides some evidence that the correlation shapes are not very sensitive to precise jet flow parameters.

IV. Acoustic source modelling and sound fields

The fourth-order two-point velocity correlations shown in Fig. 5 have a remarkably simply form. They are well approximated by a Gaussian function of the form:

$$R_{ijkl}(\mathbf{x},\boldsymbol{\Delta},\tau) = A_{ijkl}(\mathbf{x})\exp[-\Delta_1/(\bar{u}\tau_s(\mathbf{x})) - \ell n2\left((\Delta_1-\bar{u}\tau)^2+\Delta_2^2+\Delta_3^2\right)/l_s^2(\mathbf{x})]. \tag{13}$$

Such a function has been used previously, for example in Ref. 12 but here we are able to compare it with the results of a LES simulation to determine the unknown parameters. In making the comparison in Fig. 6 the values for the amplitude $A_{1111}(\mathbf{x})$, decay time scale $\tau_s(\mathbf{x})$ and Gaussian length scale $l_s(\mathbf{x})$ were chosen at each position **x** to give the best fit to the LES results. The agreement is encouraging. However, the real advantage of using an acoustic analogy lies in its application without recourse to a LES solution. So we investigate to what extent the parameters defining the source statistics, $A_{ijkl}(\mathbf{x})$, $\tau_s(\mathbf{x})$ and $l_s(\mathbf{x})$, can be determined from a much simpler and quicker RANS calculation. One might hope that [8, 11-14]

$$A_{ijkl}(\mathbf{x}) = C_{ijkl}(2\bar{\rho}k)^2, \quad l_s(\mathbf{x}) = c_l k^{3/2}/\varepsilon \quad \text{and } \tau_s(\mathbf{x}) = c_\tau k/\varepsilon, \tag{14}$$

where C_{ijlk}, c_l and c_τ are nondimensional constants and $k^{3/2}/\varepsilon$ and k/ε are the usual turbulence length and time scales arising from the RANS calculation.

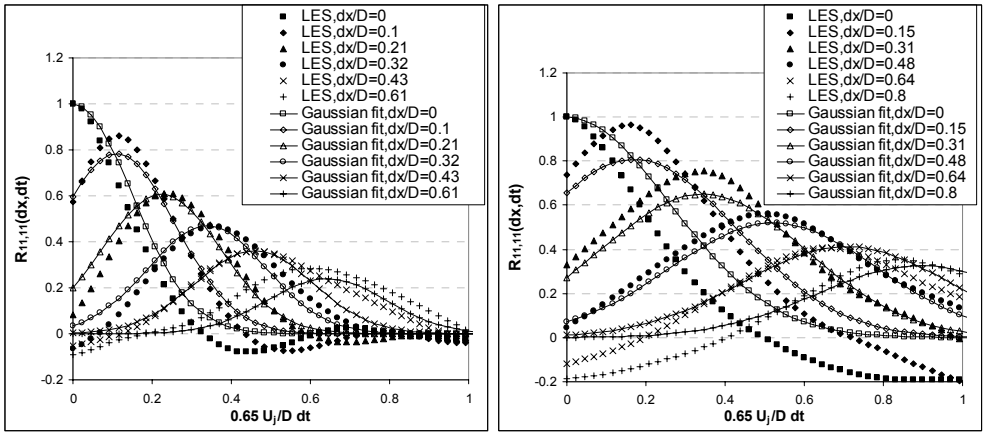

(a) (b)

Figure 6. Gaussian fitting to the LES 4th order velocity correlation results, which correspond to the shear layer location r/D= 0.5 and two axial locations downstream of the nozzle (x_1=0) at (a) x_1/D = 4 (b) x_1/D = 6.

Figure 7 shows the comparison of the parameters obtained from the best fit Gaussian with the values from RANS Case B. In making the comparison we have plotted the axial integral length scale,

$$\ell_{\text{int}}(\mathbf{x}) = \int_{-\infty}^{\infty} \exp\left[-\frac{|\Delta_1|}{\bar{u}\tau_s(\mathbf{x})} - \ell n 2 \left(\frac{\Delta_1}{l_s(\mathbf{x})} \right)^2 \right] d\Delta_1 .$$

and the autocorrelation time decay constant $\tau_S(\mathbf{x})$. We see that they are proportional the RANS length and time scales over the wide range of axial positions (from 0.7 to 6 jet diameters D downstream of the nozzle) which includes all the noise-producing regions. The amplitude comparison is made in Fig. 7c by plotting $\sqrt{C_{iijj}} = \sqrt{R_{iijj}(\mathbf{x},\mathbf{0},0))}/(2\overline{\rho}k)$. Since $R_{iijj}(\mathbf{x},\mathbf{0},0) = \overline{T'_{ii}(\mathbf{x},t)T'_{jj}(\mathbf{x},t)}$ this shows the ratio of the square-root of the autocorrelation of T'_{ii} from best-fit Gaussian with the local values of $(2\overline{\rho}k)^2$ from the RANS. We see that this ratio is approximately constant. The direct proportionality between the best fit Gaussian values and the RANS parameters means that we can, with confidence, use the RANS results in the description of acoustic sources. The excellent agreement between the fourth-order velocity correlations and experimental data at different Reynolds numbers in Fig. 5 strongly suggests that these constants are universal, but until more simulations have been made we cannot say that categorically.

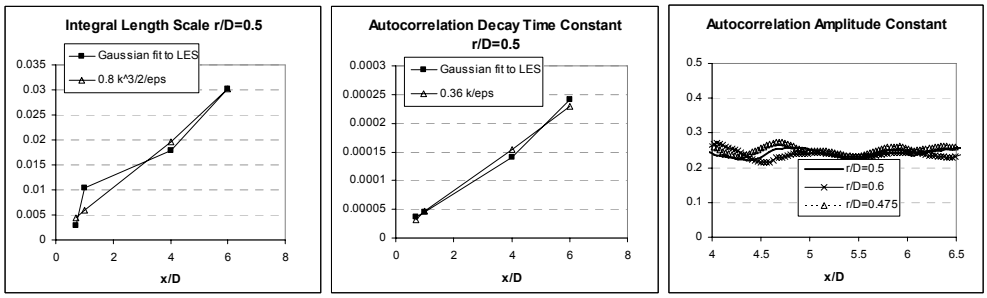

(a) (b) (c)

Figure 7. Axial variation of space, time and amplitude scales from the best-fit Gaussian to the LES results compared with scales from the RANS for different axial positions downstream of the nozzle (x_1=0), (a) integral axial length scale $\ell_{\text{int}}(\mathbf{x})$ (b) autocorrelation time decay constant, τ_s (c) $\sqrt{C_{iijj}} = \sqrt{R_{iijj}(\mathbf{x},\mathbf{0},0)}/(2\overline{\rho}k)$.

In summary, the relationship between the parameters in the Gaussian that gives the best fit to the LES and the RANS scales are

$$c_l = 0.36, c_\tau = 0.37 \text{ and } \sqrt{C_{iijj}} = 0.25. \tag{15}$$

They are compared with values used in the literature based on best fits to the far-field sound in Table 1

Table 1. Non-dimensional time, length and amplitude constants

Non-dimensional constants	Tam and Auriault[12]	Morris and Farassat[13]	Current prediction based on LES
Space scale, c_l	0.13	0.78	0.36
Time scale, c_τ	0.308	1	0.37
Amplitude scale, $\sqrt{C_{iijj}}$	0.2567	0.26	0.25

In the comparison in Fig. 7c, we have just plotted $\sqrt{C_{iijj}}$, but we can also use the LES solution to determine the relative magnitudes of all the components of R_{ijkl}. Analysis of the LES solution shows that the only significant components are R_{1111} (where 1 is the jet flow direction and 2 and 3 are in the cross-plane), R_{2222} and R_{3333} in the cross plane of the jet (with 2 circumferential and 2 radial), and the cross terms R_{1212} and R_{2323} (and the terms they are equal to by symmetry, such as R_{2112}, R_{1221} etc). Moreover their relative magnitudes are remarkably independent of position **x** within the jet (see Fig. 8). Having informed the choice of the non-dimensional constants of proportionality through comparison with the LES solution, there are no remaining undetermined empirical constants in the source description and we can obtain absolute predictions for the sound field.

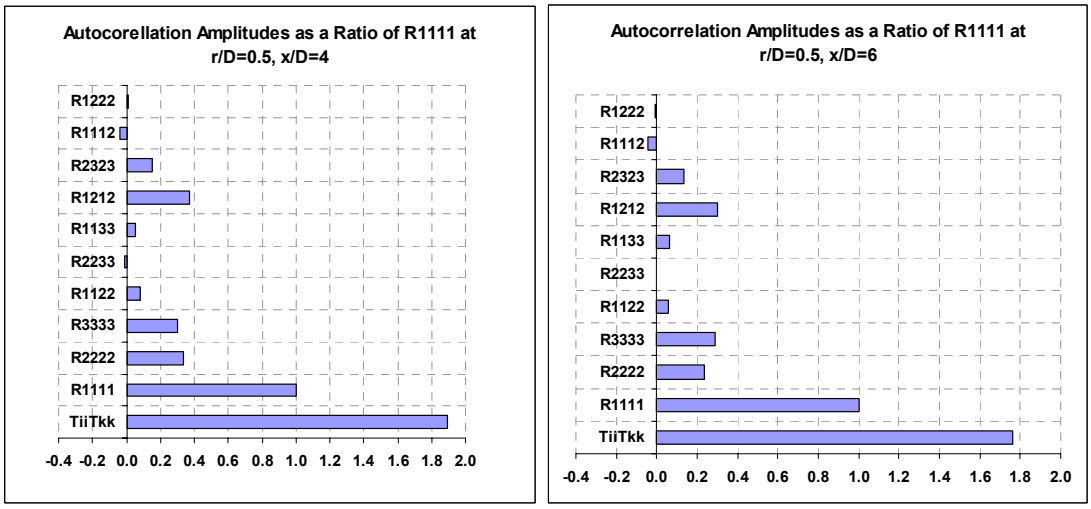

(a) (b)

Figure 8. Autocorrelation amplitudes as a ratio of $R_{1111}(\mathbf{x},0,0)$ in the shear layer location r/D = 0.5; downstream of the nozzle (x_1=0) at (a) x_1/D= 4, and (b) x_1/D = 6, the 2 direction is circumferential and the 3 radial.

In Figs 9-13, we present a summary of results for the sound obtained using the source description in equations (13) – (15). Predictions are compared to experimental results obtained in the JEAN project[19] for a hierarchy of models chosen to aid identification of the effects of source directivity. We also study the effect of the mean flow propagation model on the sound prediction. This is done by comparing a locally parallel jet approximation with propagation through a jet emerging from a nozzle, which is determined through the numerical solution of the system

of linearised Euler equations described in Section II and includes scattering by the nozzle and jet spreading. The mean flow is taken from the RANS B solution.

Results for the simplest model of propagation through a locally parallel flow and an instantaneously isotropic model of turbulence as used in Ref. 13 are shown in Fig. 9. In this source model $R_{ijkl}(\mathbf{x})$ is taken to be proportional to $\delta_{ij}\delta_{kl}$. We can write the constant of proportionality in the form:

$$R_{ijkl}(\mathbf{x}) = R_{ppqq}\delta_{ij}\delta_{kl}/9. \tag{16}$$

In making this comparison of the sound field, we have matched $R_{ppqq}(\mathbf{x})$ to the LES results by using equations (13) and (14) with $\sqrt{C_{ppqq}} = 0.25$. This gives reasonable predictions at 90 º to the jet axis but leads to a major underprediction at small angles to the jet. It should be recognised that the amplitude level in this prediction is somewhat arbitary since we are not (yet!) modelling the source direction correctly. If instead of matching $R_{ppqq}(\mathbf{x})$, we had matched $R_{1111}(\mathbf{x})$ the prediction would have been 7dB higher with its shape unchanged. Assuming statistical isotropy (ie $R_{ijkl}(\mathbf{x})$ proportional to $\delta_{ij}\delta_{kl} + \delta_{ik}\delta_{jl} + \delta_{il}\delta_{jk}$) leads to little change (Fig.10).

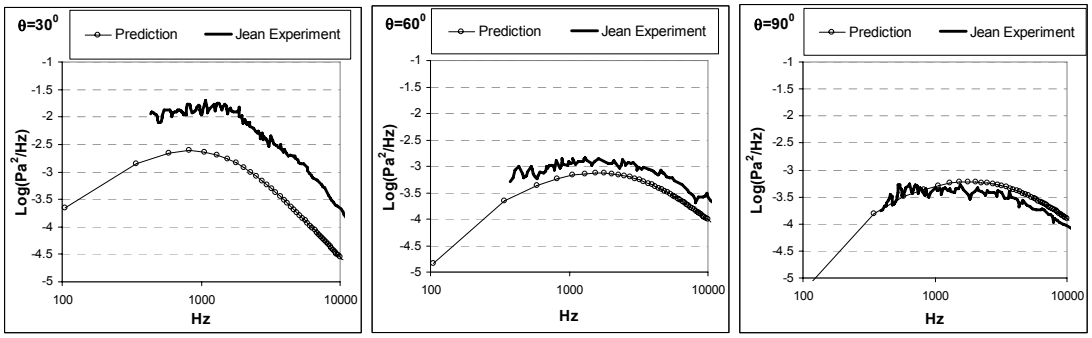

(a) (b) (c)

Figure 9. Spectra comparison with experiment at (a) $30^{0;}$ (b); 60^0 and (c) 90^0 to the jet axis for predictions based on the locally parallel jet meanflow model and the instantaneously isotropic source model based on $R_{ijkl} = R_{ppqq}\delta_{ij}\delta_{kl}/9$.

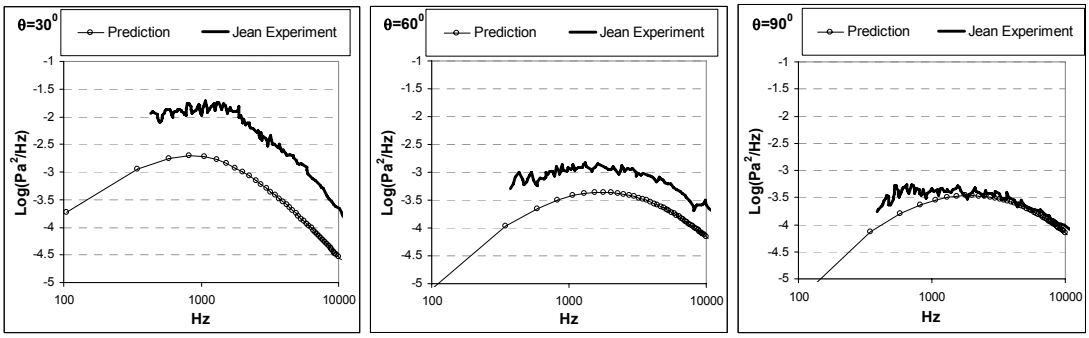

(a) (b) (c)

Figure 10. Spectra comparison with experiment at (a) 30^0 (b) 60^0 and (c) 90^0 to the jet axis for predictions based on the locally parallel jet meanflow model and the statistically isotropic source model based on $R_{ijkl} = R_{ppqq}(\delta_{ij}\delta_{kl} + \delta_{ik}\delta_{jl} + \delta_{il}\delta_{jk})/15$.

For the statistically isotropic source and the spreading jet propagation model, we have tested a few commonly made approximations. Figure 11 shows comparison between predictions for the sound obtained using a Green function for a spreading jet mean flow which includes scattering by the nozzle, with those using the far-field form of

the locally parallel flow Green function. As expected the difference is negligible at 90º to the jet axis, but is more signifcant at small angels, where it can be as much as 5dB at higher frequencies. The difference at low frequencies is mostly due to the far-field approximation made in the Green function for the locally parallel flow. This is shown explicitly in Figure 12a which compares the evolving jet Green function with that calculated when the far-field approximation is made. In the test case of the JEAN experimental data[18], the measurements were made at a radius R =30D and this turns out to be sufficiently close to the jet that the near field correction should be retained. Finally in Fig. 12b, we test the error introduced by assuming that the radial variation of the Green function and its derivatives in I_{ij} defined in equation (10) is small over the correlation length of the turbulent sources, an approximation made by Tam and Auriault[12]. The statistical isotropic source involves a shear term T'_{13} (3 is in the radial direction) which is multiplied by a propagation term $\partial G_1 / \partial r$, and since the axial velocity-like variable in the Green function, G_1, varies rapidly with radius in the shear layer it and its derivative are not necessarily negligible over a turbulent correlation length. The effect of these approximations is particularly drastic at low frequencies, for which acoustic wavelengths are about the same as the distance from the observer to the nozzle exit (Fig.12a) and and the shear source terms [14]are important in the source model (Fig.12b). In summary, for the case considered both the far-field approximation and the small radial variation of the Green function lead to inaccurate sound predictions and should be avoided.

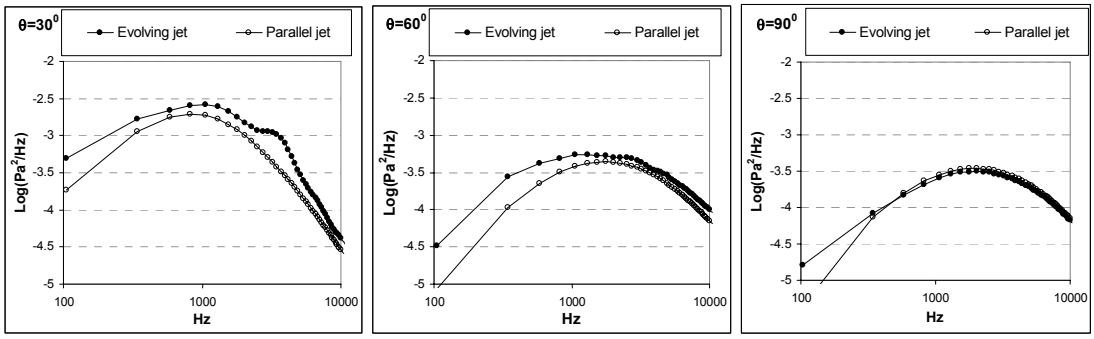

(a) (b) (c)

Figure 11. Spectra comparison at (a) 30^0 (b) 60^0 and (c) 90^0 to the jet axis for predictions based on the statistically isotropic source model and Green functions describing propagation through an evolving jet meanflow and the locally parallel meanflow respectively.

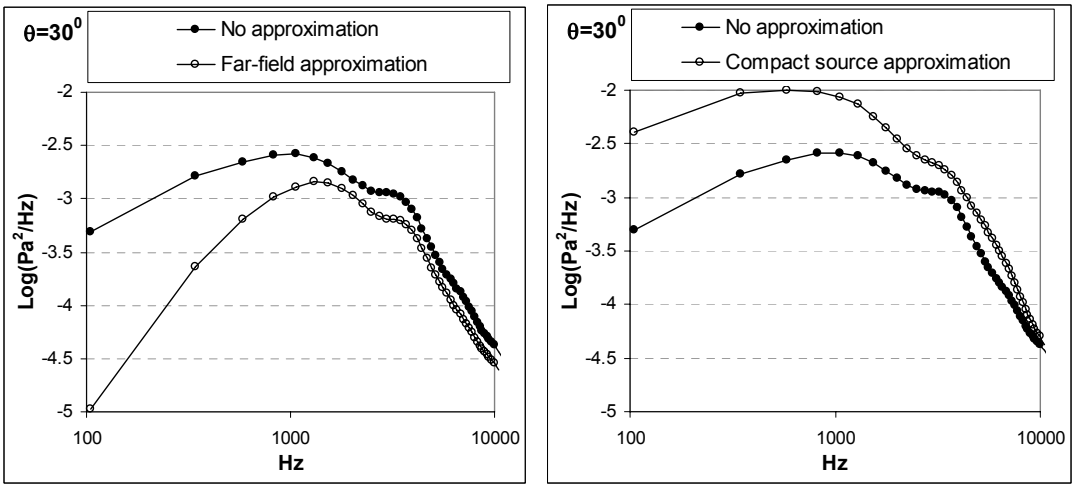

(a) (b)

Figure 12. Effect of further approximations for the evolving jet meanflow model and the statistically isotropic source model on the spectra prediction for the observer position at 30^0 to the jet, (a) assuming the far-field form of the Green's function; and (b) neglecting the radial variation of the Green's function over the correlation length of the turbulent source.

The results in Fig. 8 show clearly the anisotropy in the acoustic sources and so we should not be surprised that the sound field predicted from the isotropic source models in Figs. 9-12 are unable to capture the sound correctly. We now consider a more realistic source directivity informed by the relative magnitudes of the different components in the LES. Then a much improved prediction is obtained which, as shown in Fig 14, is within 2dB of the experimental data for all angles. This is the main result of this paper. In these plots a frequency of 5kHz corresponds to a Strouhal number of 1. It should be emphasised that there are no empirical constants in the description of the acoustic source terms, which are determined by the RANS solution with constants of proportionality determined entirely using data extracted from the near-field LES results. Although only the main source components have been included in these plots (R_{1111}, R_{2222}, R_{3333} , R_{1212} and R_{2323} (and terms equal to these from symmetry), where 2 is circumferential and 3 radial), the remaining terms are so small that there is no difference in the predicted spectrum if all source components are included with their relative amplitudes as determined from the LES results.

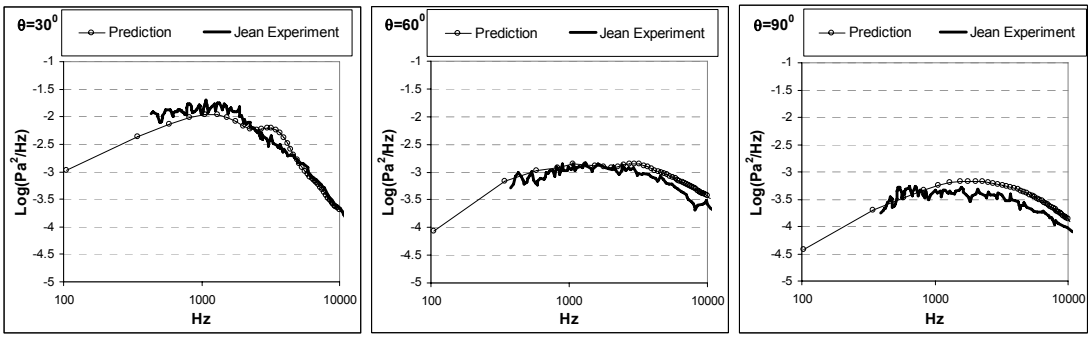

(a) (b) (c)

Figure 13. Spectra comparison with experiment at (a) 30^0 (b) 60^0 and (c) 90^0 to the jet axis for predictions based on a Green function for an evolving jet meanflow and the axisymmetric anisotropic source model.

One advantage of deriving the sound field through a representation theorem in this way is that, since the far-field sound is obtained by integrating the product of the Green function and the source, it is possible to identify the jet locations that contribute most to the sound at different frequencies. Sample results are shown in Figs. 14 and 15. As expected, as the frequency increases the most significant sound producing zone in the jet moves upstream towards the nozzle exit. For angles close to the jet and the peak sound frequency St=0.2, the most significant source location is just downstream of the potential core of the jet in the shear layer.

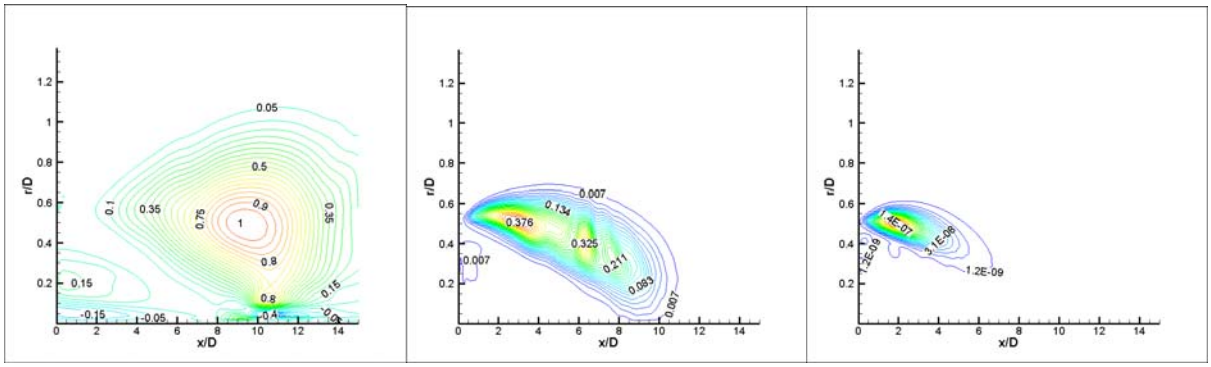

(a) (b) (c)

Figure 14. Contours of contributions to spectral density, i.e. the inner convolution product of the propagation operator based on the Green function and the source function based on the statistically isotropic model and the Gaussian source description normalised by the peak sound value, for the observer location at 30^0 to the jet, which demonstrate locations in the jet, which are contribute most to the sound spectra at different frequencies: (a) St=0.2 (peak sound) (b) St=1 (c) St=2 .

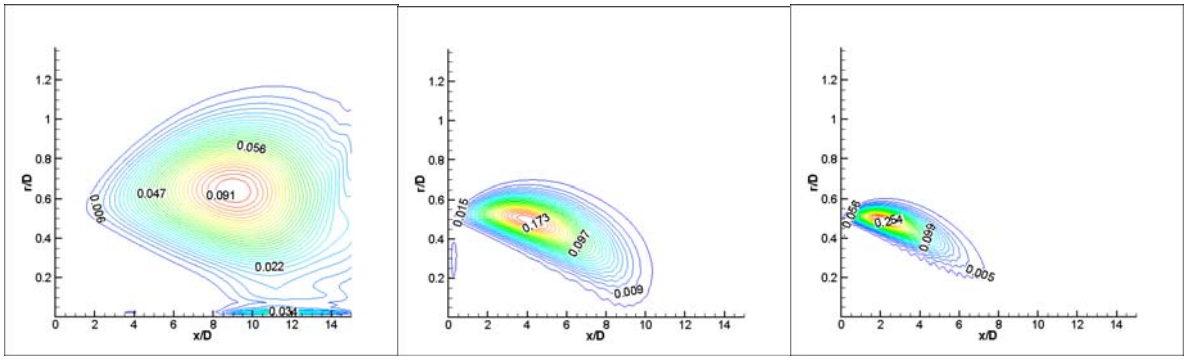

Figure 15. As Fig. 14 but for an observer location at 90^0 to the jet

V. Conclusion

We have developed a simple prediction methodology for jet noise. The approach is a hybrid one made up of three components, with each component using modelling and numerical techniques optimised to suit a particular purpose. The propagation of noise to the far field is captured via a solution of the adjoint Linearised Euler Equations (LEE) to determine the adjoint Green function describing how sound emitted by the jet is modified by propagation through the time-averaged but spatially developing jet flow field. The sound generation is described by Goldstein's acoustic analogy. A Gaussian function is used to model the cross-correlation of the fourth-order velocity fluctuations which are the main acoustic sources in an isothermal jet, and the parameters describing their amplitude, length and time scales are taken to be proportional to the local square of the kinetic energy, the length and timescales from a RANS solution. We have determined the constants of proportionality through comparison with correlations obtained from LES. Comparison has also been made with an experiment at a different Reynolds number and the constants appear to be universal. The LES results have been used to determine the relative magnitudes of the various components of the acoustic sources and only a few terms are found to be significant. The fourth-order correlation of the axial velocity R_{1111} is approximately 3 times R_{2222} and R_{3333}, and the radial component R_{3333} tends to be slightly larger than the tangential term R_{2222}. In addition to these components, R_{1212} and R_{2323} are also significant. The ratio of the relative magnitude of the various components in the source is found not to change with position in the jet. Thus informed by the LES solution, the source description is determined with *no empirical constants*. The far-field sound is then predicted through an integration of the Green function with this acoustic source. Comparison between this predicted noise and the JEAN[19] experimental data gives excellent agreement across a wide spectral range, even at angles close to the jet axis. Investigation of the integrand determines the regions of the jet that contributes most to the sound field at different frequencies and observer positions.

We have used the methodology to determine the accuracy of some commonly made approximations. These include:

i) the effect of jet evolution and scattering by the nozzle on the sound propagation

This was determined by comparison of results using of numerically determined Green function with that calculated analytically for a locally parallel mean flow. As one would expect, it has little effect near 90º to the jet axis but it can be significant at shallow angles. In the example considered of a 0.75 Mach number isothermal jet, it led to a difference of about 5 dB at 30º to the jet axis for high frequencies.

ii) isotropic source models used previously in the literature

We have found significant differences in the far-field sound according to the assumed relative values of the components of the turbulent sources Analysis of the LES results has shown that the sources are far from isotropic. However only a few components are significant and their ratios as determined from the LES results appear to be independent of position in the jet. When the ratio of components from the LES solution is used in the source description the predicted sound agrees well with experimental data for all frequencies and angles.

iii) the assumption that the radial variation of Green's function is small over the correlation length of the turbulent sources

When the sources have non-zero shear terms eg T'_{13} are nonzero, the propagation terms involve the radial derivative of the axial adjoint velocity variable. This varies rapidly across the shear layer of the jet boundary and cannot be assumed to be uniform across the correlation length of the turbulent sources. To assume that it is can lead to errors of in excess of 6dB.

iv) *the far-field form*

For the experimental data set we were using the experimental data at *R/D*=30 is sufficiently close to the jet that making a far-field approximation in the Green function leads to large errors in the spectral density at mid and low frequencies (for example an error of 3dB at 1kHz) where the acoustic wavelengths are about the same as the distance of the measurement position from the nozzle exit. The near field correction should be included in the calculation of the Green function.

Acknowledgments

This research was funded by the Engineering and Physical Sciences Research Council, and carried out in collaboration with Rolls-Royce plc. Their support and interest is gratefully acknowledged. The second set of RANS calculations were performed by Olivier Marsden and Elena de la Rosa Blanco helped with the analysis of the LES results.

References

[1]Lighthill, M.J., "On sound generated aerodynamically: I. General theory," Proceedings of the Royal Society of London A, **222**, 1952, pp. 564-587.

[2]Ffowcs Williams, J. E., "The noise from turbulence convected at high speed" *Phil Trans Roy Soc. Lond*. **255**, 1963, pp 469-503.

[3]Dowling, A. P., Ffowcs Williams, J. E., and Goldstein, M. E., "Sound production in a moving stream". *Phil Trans. Roy. Soc. Lond*., A **288**, 1978, pp 321-349.

[4]Mani, R., "The influence of jet flow on jet noise," Parts 1 and 2. *J. Fluid Mech*., **73**, 1976, pp 753-793.

[5]Lilley, G. M., "On the noise from jets," *Noise Mechanism*s, CP-131-Agard, 1974, 113.1-13.12.

[6]Colonius, T., Lele, S. K., and Moin, P., "Sound generation in a mixing layer," *J. Fluid Mech*., **330**, 1997, pp 375-409.

[7]Goldstein, M.E., "A generalized acoustic analogy," *J. Fluid Mech*., **488**, 2003 pp 315-333.

[8]Tam, C.K.W., and Auriault, L., "Mean flow refraction effects on sound radiated from localized sources in a jet," *J. Fluid Mech*., **370**, 1998, pp. 149-174.

[9]Argawal, A., Morris P.J., and Mani, R., "Sound propagation in non-uniform flows: Suppression of instability waves," *AIAA Journal*, **42**, 2004, pp 80-88.

[10]Karabasov, S. A. and Hynes, T. P., "Adjoint Linearized Euler solver in the frequency domain for jet noise modelling," AIAA-2006-2673 *12th AIAA/CEAS Cambridge, Massachusetts*, 2006

[11]Bechara, W., Lafon, P., Bailly, C., and Candel, S. M., "Application of a k-ε turbulence model to the prediction of noise for simple and coaxial free jets", *J. Acoust. Soc. Am*. **97**, 1995, pp 3518-3531.

[12]Tam, C.K.W., and Auriault, L., "Jet mixing noise from fine scale turbulence," AIAA Journal, **206**, No. 2, 1999, pp 145-153.

[13]Morris, P.J., and Farassat, F., "Acoustic analogy and alternative theories for jet noise prediction," *AIAA Journal*, **40**, 2002, pp 671-680

[14]Afsar, M.Z., Dowling, A.P., and Karabasov, S.A., "Jet noise in the zone of silence," AIAA-2007-3606, 13th *AIAA/CEAS Aeroacoustics Conference*, Rome, Italy, May 2007.

[15]Page, G. J., Zhao, H., and McGuirk, J. J., "A parallel multi-block Reynolds-Averaged Navier-Stokes method for propulsion installation application", *12th International Symposium on Air Breathing Engines*, **1**, 1991, pp. 864 –876.

[16]Page, G. J., Li, Q., and McGuirk, J. J., "LES of impinging jet flows relevant to vertical landing aircraft," AIAA-2005–5226, *23rd AIAA Applied Aerodynamics Conf.*, Toronto, Canada, June 2005..

[17]Power, O., Kerherve, F., Fitzpatrick, J., and Jordan, P., "Measurements of turbulence statistics in high subsonic jets", AIAA-2004-3021, *10th AIAA/CEAS Aeroacoustics Conference,* Manchester, UK, June 2004.

[18]ERCOFTAC Special Interest Group on Quality and Trust in industrial CFD, Best Practice Guidelines 1999

[19]Hollis, D., "Particle Image Velocimetry in gas turbine combustor flow fields" *PhD Thesis, Loughborough University*, 2004.

[20]Harper-Bourne, M., "Jet noise turbulence measurements", AIAA-2003-3214, *9th AIAA/CEAS Aeroacoustics Conference*, 2003.